Jefferson Lab PAC 44

Nuclear Exclusive and Semi-inclusive Measurements with a New CLAS12 Low Energy Recoil Tracker

ALERT Run Group[†]

EXECUTIVE SUMMARY

In this run group, we propose a comprehensive physics program to investigate the fundamental structure of the ^{4}He nucleus. An important focus of this program is the study of the partonic structure of bound nucleons. To this end, we propose next generation nuclear measurements in which low energy recoil nuclei are detected. Tagging of recoil nuclei in deep inelastic reactions is a powerful technique that will provide unique information about the nature of medium modifications, through the measurement of the EMC ratio and its dependence on the nucleon off-shellness. Other important channels are the coherent exclusive Deep Virtual Compton Scattering (DVCS) and Deep Virtual Meson Production (DVMP) with a focus on the ϕ meson. These are particularly powerful tools enabling model-independent nuclear 3D tomography through the access of partons' position in the transverse plane. These exclusive measurements will also be used to study the generalized EMC effect and for the first time access the gluonic tomography of nuclei via exclusive ϕ electroproduction channel. Finally, we propose to measure tagged DVCS on light nuclei (d, ^{4}He) to extract both quasi-free neutron and bound neutron and proton Generalized Parton Distributions (GPDs). In both cases, the objective is to study nuclear effects and their manifestation in GPDs including the effect of final state interactions in the measurements of the bound nucleon beam spin asymmetries and the EMC ratio.

At the heart of this program is the Low Energy Recoil Tracker (ALERT) combined with the CLAS12 detector. The ALERT detector is composed of a stereo drift chamber for track reconstruction and an array of scintillators for particle identification. Coupling these two types of fast detectors will allow ALERT to be included in the trigger for efficient background rejection, while keeping the material budget as low as possible for low energy particle

[†]Contact Person: Kawtar Hafidi (kawtar@anl.gov)

detection. ALERT will be installed inside the solenoid magnet instead of the CLAS12 Silicon Vertex Tracker. We will use an 11 GeV longitudinally polarized electron beam (80% polarization) of 150 nA on a gas target straw filled with deuterium or ^{4}He at 3 atm to obtain a luminosity of 3.10^{34} cm^{-2}s^{-1}. In addition we will need to run hydrogen and ^{4}He targets at different beam energies for detector calibration. The following table summarizes our beam time request:

Measurements	**Particles detected**	**Targets**	**Beam time request**	**Luminosity***
ALERT Commissioning	p, d, ^{4}He	H and He	5 days	Various
Tagged EMC	p, ^{3}H, ^{3}He	^{2}H and He	$20 + 20$ days	3.10^{34} cm^{-2}s^{-1}
Tagged DVCS	p, ^{3}H, ^{3}He	^{2}H and He	$20 + 20$ days	3.10^{34} cm^{-2}s^{-1}
Nuclear GPDs	^{4}He	He	extra 10 days on He	6.10^{34} cm^{-2}s^{-1}
Additional Topics	p, d, ^{3}H, ^{3}He	^{2}H and He	$20 + 20 + (10)$ days	$3(6).10^{34}$ cm^{-2}s^{-1}
TOTAL			**55 days**	

*This luminosity value is based on the effective part of the target. When accounting for the target's windows, which are outside of the ALERT detector, it is increased by 60%

Other Physics Opportunities with the ALERT Run Group

W. Armstrong[†], J. Arrington, I. Cloet, K. Hafidi[†‡], M. Hattawy[†], D. Potteveld, P. Reimer, Z. Yi

Argonne National Laboratory, Lemont, IL 60439, USA

J. Bettane, G. Charles, R. Dupré[†], M. Guidal, D. Marchand, C. Muñoz, S. Niccolai, E. Voutier

Institut de Physique Nucléaire, CNRS-IN2P3, Univ. Paris-Sud, Université Paris-Saclay, 91406 Orsay Cedex, France

M. J. Amaryan, G. Dodge

Old Dominion University, Norfolk, VA 23529, USA

N. Baltzell, S. Stepanyan

Thomas Jefferson National Accelerator Facility, Newport News, VA 23606, USA

S. Joosten, Z. E. Meziani, M. Paolone

Temple University, Philadelphia, PA 19122, USA

S. Liuti

University of Virginia, Charlottesville, VA 22903, USA

[†]Spokesperson

[‡]Contact person: kawtar@anl.gov

Abstract

This proposal summarizes additional physics measurements that can be done as part of the ALERT run group without need for a new beam time. There is a tremendous potential for this data, which can advance our understanding of QCD on several fronts including the structure of nucleons and nuclei, the modification of hadron structure in the nuclear medium, the final state interaction and meson spectroscopy. The key to achieving success in all these areas is the detection of the recoil fragments. This can be achieved with the newly proposed low energy recoil tracker (ALERT).

As a complementary measurement to "the partonic structure of light nuclei" proposal, which focuses on deep virtual Compton scattering (DVCS) off ^{4}He nucleus, we propose to extend the measurement to deuteron. This will allow us and for the first time to measure in exclusive way DVCS off deuterium to shed light on its partonic structure. For deep virtual meson production (DVMP) measurements, we would like to extend the ϕ measurements to the π^0 meson, which will allow access to the ^{4}He single chiral-odd GPD H_T. Finally, we propose to measure DVCS in three-body break up reactions, which will be a natural extension of the "Tagged DVCS off light nuclei" proposal.

This fourth proposal shows our every intention to fully exploit the data collected during the ALERT run group because of its uniqueness and the potential it has to enable breakthroughs in our understanding of nuclear QCD.

Contents

Introduction

The combination of the high luminosity available at Jefferson Lab, the large acceptance of CLAS12 detector and the low energy recoil tracker (ALERT) offers an amazing opportunity to advance our understanding of long standing mysteries in nuclear QCD such as the EMC effect. Moreover, the ability to detect low energy recoil fragments or what we also call the fragment tagging technique is crucial to control final state interactions (FSI) which spoil most of the semi-inclusive measurements.

This new development in detection capabilities, will allow the study of medium modification free from fermi motion uncertainties and FSI effects. It is therefore clear that the focus of the three main proposals of the ALERT run group is only a fraction of the physics that can be achieved by successfully analyzing the ALERT run group data. This data will be a gold mine, which will allow us to investigate in a unique way several important physics questions and conquer new territories in the nuclear QCD land. These are examples of physics that can be studied with the ALERT data. Some of the topics were included in the JLab letter of intent LOI-10-009 [1] submitted to PAC35:

- Coherent DVCS and DVMP off deuteron. For DVMP, we can study for example π^0, ϕ, ω and ρ mesons.
- Deep virtual π^0 production off ^{4}He, which is interesting by itself but also the background of DVCS measurements.
- Semi-inclusive reaction p(e,e'p)X to study the π^0 cloud of the proton and $D(e, e'pp_S)X$ to study the π^- cloud of the neutron, at very low proton momenta.
- Meson spectroscopy in coherent production off ^{4}He as an extension of the exploratory measurements during eg6 experiment E-07-009. Coherent production is used to eliminate physics background arising from associated baryon resonance production. In order to ensure coherent production of a mesonic state, the recoil nuclei must be detected.
- Tagged nuclear form factors measurements.
- The role of Δs in short-range correlations.

- The role of the final state interaction in hadronization and medium modified fragmentation functions.
- The medium modification of the transverse momentum dependent parton distributions.

For practical reasons, we are focusing here on three topics only. These are closely connected to the three proposals, which form the ALERT run group. These topics are exclusive π^0 production off ^{4}He, coherent exclusive DVCS off deuteron and DVCS in three-body break up reactions.

Chapter 1

Summary of Physics Topics

In this proposal we briefly discuss three physics topics that can be studied using the same data as ALERT run group. These topics were chosen due to the direct relevance to the three proposed measurements which form the core of the ALERT run group.

1.1 Exclusive π^0 production off ^{4}He

A wealth of information on the QCD structure of hadrons lies in the correlations between the momentum and spatial degrees of freedom of the constituent partons. Such correlations are accessible via GPDs which, more specifically, describe the longitudinal momentum distribution of a parton located at any given position in the plane transverse to the longitudinal momentum of the fast moving nucleon. Various GPDs extracted from measurements of hard exclusive reactions with various probe helicities and target spin configurations are necessary to identify this subset of the hadronic phase-space distribution, known as the Wigner distribution. The processes which are most directly related to GPDs are DVCS and DVMP corresponding to the exclusive electroproduction of a real photon or a meson in the final state, respectively.

GPDs provide essential information for determining the missing component to the nucleon *longitudinal* spin sum rule in the kinematic setting where the proton moves in the z direction, its spin being polarized along the same direction. A complete description of nucleon structure requires, however, understanding also the *transverse* spin ([2] and references therein). An experimental determination of the chiral-odd quark helicity-flip GPDs, $H_T(x,\xi,t), E_T(x,\xi,t), \tilde{H}_T(x,\xi,t)$, and $\tilde{E}_T(x,\xi,t)$ [3] is crucial for this effort.

In Ref.[4], it was suggested that deeply virtual exclusive pseudoscalar electroproduction can provide a direct channel to measure chiral-odd GPDs so long as the helicity flip contribution to the quark-pion vertex is dominant. This idea was subsequently endorsed and further developed in Refs.[5, 6, 7, 8, 9]. Recently, experimental measurements from

Jefferson Lab have been interpreted in terms of chiral odd GPDs [10, 11, 12]. In particular, by measuring separately π^o and η production [11], it is possible to perform a flavor separated analysis of the chiral odd GPDs. As pointed out in [7, 13], however, in principle all four chiral odd GPDs enter the description of the various terms in the nucleon cross section. It is therefore a tantalizing job to disentangle their various contributions.

The number of GPDs needed to parametrize the partonic structure of a nucleus depends on the different configurations between the spin of the nucleus and the helicity direction of the struck quark. For example, for a target of spin s, the number of chiral-even GPDs is equal to $(2s+1)^2$ for each quark flavor. DVCS off spinless nuclear targets, such as ^{4}He, ^{12}C and ^{16}O, is simpler to study since only a chiral-even GPD, H_A, and a chiral-odd GPD, H_A^T, are present at leading twist and two chiral even GPDs, $H_A^{(3)}$, and $\tilde{H}_A^{(3)}$, arise at twist three.

The ^{4}He nucleus, characterized by its high density can be considered as the smallest of complex nuclei. Moreover, inclusive scattering off ^{4}He shows a large EMC effect. Therefore, this nucleus represents an ideal target for understanding a variety of nuclear effects through GPDs measurements. The twist three GPDs, $H_A^{(3)}$ and $\tilde{H}_A^{(3)}$, allow us to access the so far unexplored spin correlation of a longitudinally polarized quark in an unpolarized target. This, in turn, would give us unique information on the quark spin-orbit interaction, $\vec{S}\cdot\vec{L}$, in a nuclear environment [14]. We recall, again, that for a spin zero target the twist three GPDs are much easier to disentangle than in a nucleon, since the description of the latter requires a larger number of functions. The chiral-odd GPD, H_A^T, measured through deeply virtual π^0 production (background to DVCS signal) can be expressed in the low ξ approximation, as a convolution over the transversity GPD, H_T. The latter becomes the transversity PDF, h_1, in the forward limit. Measurements of nuclear medium modifications of this quantity would be crucial for further exploring the hypothesis originally put forward in Ref.[15] of whether the EMC effect is enhanced in spin dependent observables.

We propose to measure coherent deep exclusive π^0 BSA off ^{4}He to extract both the real and imaginary part of chiral-odd nuclear Compton form factors H_A^T and investigate the sensitivity to twist-3 contributions. The corresponding formalism is described in details in Appendix A.

1.2 Coherent exclusive DVCS off deuteron

Deep inelastic scattering processes in the deuteron have been used mainly as the source of information on unpolarized and polarized distributions of a neutron in the forward limit. With the advent of DVCS it became possible to study GPDs of a deuteron as a whole leaving it intact in the final state. Due to the fact that it is a spin-1 object, there are entirely new functions appearing, which could give us a deeper understanding of this nucleus in terms of its fundamental degrees of freedom. The nine GPDs for a spin-1 object have

been given in Ref.[16] and their properties have been discussed in detail in Ref.[17]. Sum rules relate these GPDs to the usual deuteron form factors $G_i(i = 1, 3)$, which are linear combinations of charge monopole G_C, magnetic dipole G_M , and charge quadrupole, G_Q. The unique feature of these relations is the fact that $G_3(t)$ form factor is totally dominated by the charge quadrupole $G_Q(t)$ [18] and allows us to access the H_3 GPD via beam-spin asymmetry measurements. This will be the first measurement of the partonic structure function of the deuteron related in the forward limit to charge quadrupole, and not only to charge and magnetic form factors, which can not be decomposed into simple additive sum of the proton and neutron. Using the results of these measurements we can access the partonic structure of the deuteron treated as a single hadron, which is irreducible to the partonic structure of its nucleon constituents.

We propose here to measure the beam-spin asymmetries of the coherent DVCS scattering process on deuteron target using CLAS12 to detect the scattered electron and the high energy photon and the ALERT detector to detect low energy recoil deuterons.

1.3 DVCS in three-body break up reactions

The three-body break up (3BBU) reactions are of particular interest in nuclear physics because they provide information about the substructure and nucleon correlations within a nucleus. For example quasi-elastic knock-out of neutron from ^{4}He leaves the remaining three nucleon system behind but the degree to which it remains a ^{3}He (within the PWIA) depends on the initial configuration. If the struck nucleon, *e.g.* a proton, was in a proton-triton configuration, as shown in Fig. 1.1, it seems likely that a recoil triton would be detected assuming the PWIA holds. However, if the nucleus were in a d-d configuration, a knock-out nucleon leaves behind its partner nucleon and the correlated deuteron system. This leads to a three-body break up (see Fig. 1.2) of the spectator system into a nucleon and deuteron. By fully detecting the spectator recoils we can identify the specific configuration being probed in the reaction at the event level.

Like the "Tagged DVCS" proposal of this run group, extending quasi-elastic knock-out to deeply virtual Compton scattering knock-out, we find that the DVCS reaction provides an excellent handle on final state interactions. Furthermore, unlike quasi-elastic knock-out it provides a parton level sensitivity. This partonic level measurement can be used to access not only the parton distributions of the bound nucleon, but also the parton distributions for specific configurations of the nucleus. This can be understood by considering the relative motion of correlated pairs inside of the ^{4}He nucleus as shown in Fig. 1.3. As a consequence of the N-N potential for nuclei with A $>$ 3, there is another regime of nucleon momenta that DVCS can map out to provide a picture of of the quark distributions in nucleons in different nuclear states.

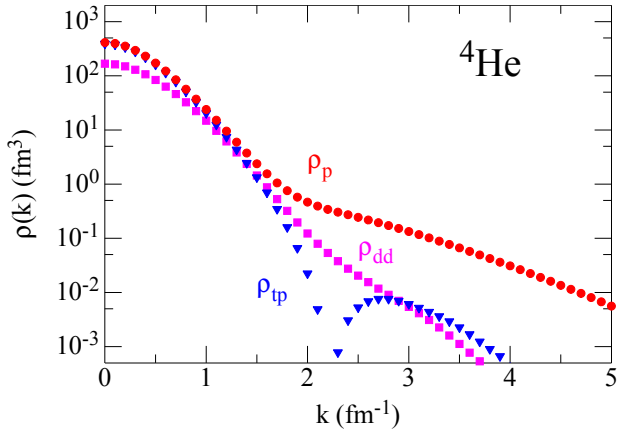

Figure 1.1: The proton momentum distribution in ^{4}He is shown by the red circles; the *tp* cluster distribution is shown by the blue triangles and the *dd* cluster distribution is shown by the magenta squares. [19]

We propose here to measure the beam-spin asymmetries of the DVCS scattering in three-body break up reactions off ^{4}He target using CLAS12 to detect the scattered electron and the high energy photon and the ALERT detector to detect low energy recoil fragments.

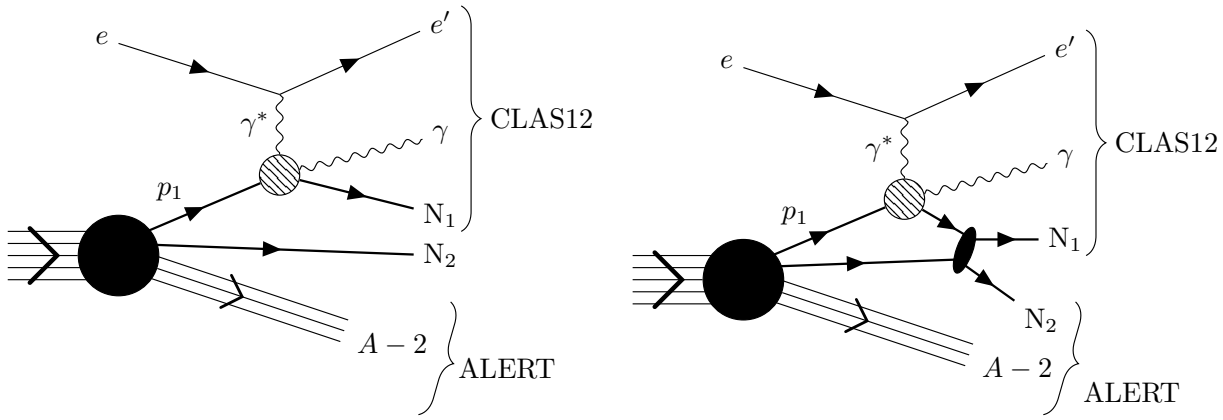

Figure 1.2: PWIA diagram for incoherent DVCS on the ^4He with 3BBU (left) and with the inclusion of final state interactions (right).

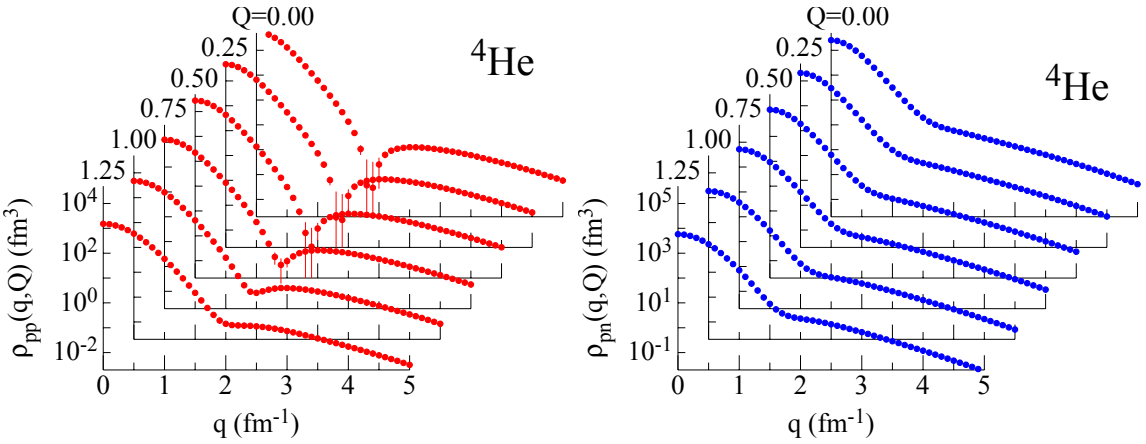

Figure 1.3: The proton-proton (left) and proton-neutron (right) momentum distributions in ^{4}He averaged over the directions of $\boldsymbol{q} = (\boldsymbol{k}_1 - \boldsymbol{k}_2)/2$ and $\boldsymbol{Q} = \boldsymbol{k}_1 + \boldsymbol{k}_2$ as a function of q for several fixed values of Q. Reproduced from Ref. [19].

Chapter 2

Experimental Setup

The different measurements of the ALERT run group require large kinematic coverage and the ability to identify the different nuclear species properly. The CLAS12 detector augmented by a low energy recoil detector is key for the success of such measurements. We summarize in Table 2.1 the requirements for the different experiments proposed in the run group.

This chapter will begin with a description of CLAS12 and the ALERT detector. After presenting the details of this new detector system, we will present an overview of the BoNuS12 RTPC followed by a discussion of how already approved or existing detectors do not satisfy the requirements for our run group.

Measurement	Particles detected	$p_{threshold}$	θ_{max}
Tagged EMC	p, ^{3}H, ^{3}He	As low as possible	As close to π as possible
Tagged DVCS	p, ^{3}H, ^{3}He	As low as possible	As close to π as possible
Nuclear GPDs	^{4}He	$230 < p < 400 MeV/c$	$\pi/4 < \theta < \pi/2$ rad

Table 2.1: Requirements for the detection of low momentum spectators fragments of the proposed measurements.

2.1 The CLAS12 Forward Detector

The CLAS12 detector is designed to operate with 11 GeV beam at an electron-nucleon luminosity of $\mathcal{L} = 1 \times 10^{35}$ cm^{-2}s^{-1}. The baseline configuration of the CLAS12 detector consists of the Forward Detector and the Central Detector packages [20] (see Fig. 2.1).

The scattered electrons will be detected in the forward detector which consists of the High Threshold Cherenkov Counters (HTCC), Drift Chambers (DC), the Low Threshold

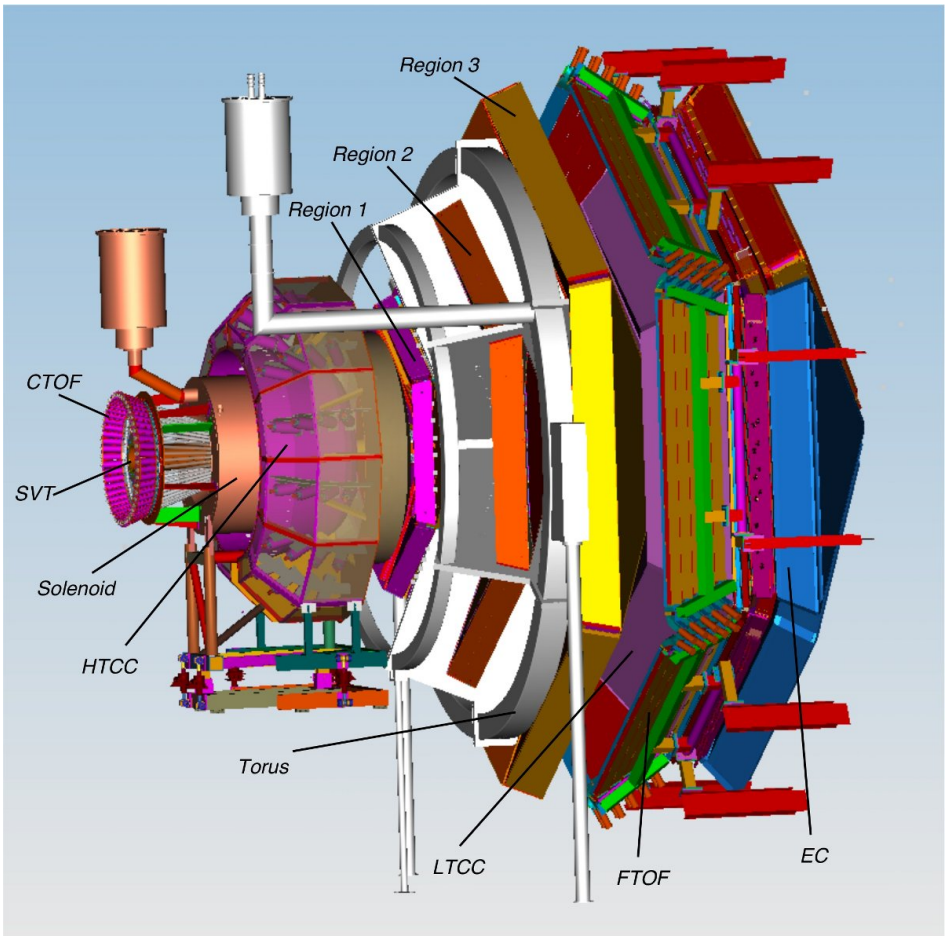

Figure 2.1: The schematic layout of the CLAS12 baseline design.

Cherenkov Counters (LTCC), the Time-of-Flight scintillators (TOF), the Forward Calorimeter and the Preshower Calorimeter. The charged particle identification in the forward detector is achieved by utilizing the combination of the HTCC, LTCC and TOF arrays with the tracking information from the Drift Chambers. The HTCC together with the Forward Calorimeter and the Preshower Calorimeter will provide a pion rejection factor of more than 2000 up to a momentum of 4.9 GeV, and a rejection factor of 100 above 4.9 GeV/c.

2.2 Design of the ALERT Detector

We propose to build a low energy recoil detector consisting of two sub-systems: a drift chamber and a scintillator hodoscope. The drift chamber will be composed of 8 layers of sense wires to provide track information while the scintillators will primarily provide particle identification. To reduce the material budget, thus pushing the energy threshold for detecting recoil particles as low as possible, the scintillator hodoscope will be placed inside the chamber, just outside of the last layer of drift wires. The good time resolution, and therefore position resolution, of the drift chamber, when coupled with the scintillators, will provide energy loss, timing, and azimuthal angle measurements for a sizable fraction of recoil particles.

The drift chamber volume will be filled with a light gas mixture (90% He and 10% C_4H_{10}) in order to not be sensitive to relativistic particles (*i.e.* electrons, gammas) and neutron backgrounds. Furthermore, a light gas mixture will increase the drift speed of electrons created during the ionization. This allows the chamber to withstand higher rates due to a shorter hit occupancy time window. The gas will likely be at atmospheric pressure but we plan to evaluate the possibility of working at a lower pressure. Based on these characteristics, the signals from this chamber and the scintillators will be used as an independent trigger, thus, reducing the DAQ trigger rate and allowing for operation at increased luminosity.

The detector must be designed to fit inside the outermost layer of Micromegas; the silicon vertex tracker and the remaining layers of Micromegas will be removed. The available space has thus an outer radius of 20 cm. A schematic layout of the preliminary design is shown in Fig. 2.2. The different detection elements are all covering about 340° of the polar angle to leave room for mechanics, and are 30 cm long with an effort made to reduce the particle energy loss through the materials. It is composed of:

- a cylindrical target, that compared to the eg6 run, is longer ($\sim$ 30 cm), wider (outer radius is 6 mm) and operating with lower pressure ($\sim$3 atm) in order to use a thinner target wall ($\sim$25μm Kapton) [1];

[1] During the eg6 run, the pressure of the drift gas in the RTPC was $\sim$ 1 atm, and the pressure of the target was $\sim$ 6.5 atm. Recent tests from S. Christo (JLab) demonstrated the feasibility of a 3 atm target with a 30 μm wall, including safety margins.

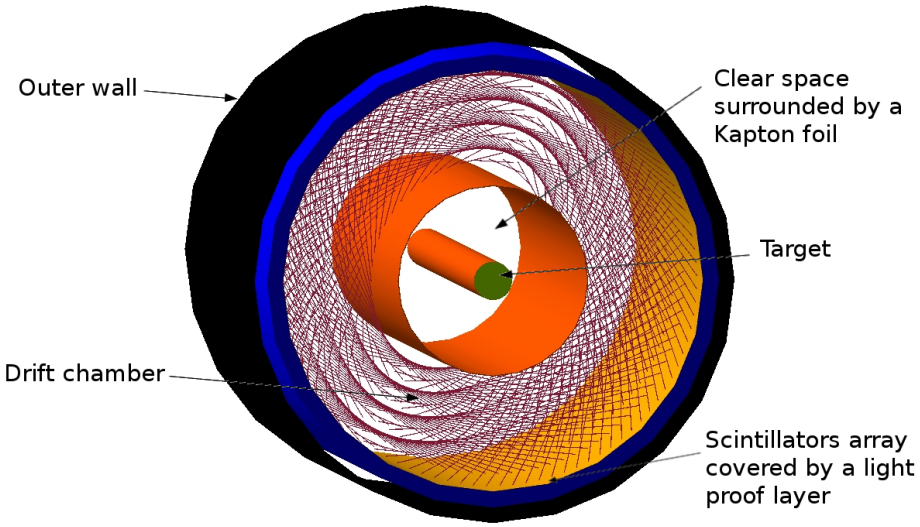

Figure 2.2: The schematic layout of the ALERT detector design, viewed from the beam direction.

- a clear space filled with helium to reduce secondary scattering from the high rate Moller electrons. Its outer radius is 30 mm;
- the drift chamber, its inner radius is 32 mm and its outer radius is 85 mm. It will detect the trajectory of the low energy nuclear recoils;
- two rings of plastic scintillators placed inside the gaseous chamber, with total thickness of roughly 20 mm.

2.2.1 The Drift Chamber

While drift chambers are very useful to cover large areas at a moderate price, huge progress has been made in terms of the ability to withstand higher rates using better electronics, shorter distance between wires and optimization of the electric field over pressure ratio. Our design is based on other chambers developed recently. For example for the dimuon arm of ALICE at CERN, drift chambers with cathode planes were built in Orsay [21]. The gap between sense wires is 2.1 mm and the distance between two cathode planes is also 2.1 mm, the wires are stretched over about 1 m. Belle II is building a cylindrical drift chamber very similar to what is needed for this experiment and for which the space between wires is around 2.5 mm [22]. Finally, a drift chamber with wire gaps of 1 mm is being built for the small wheel of ATLAS at CERN [23]. The cylindrical drift chamber proposed for our experiment is 300 mm long, and we therefore considered that a 2 mm gap between wires was technically a rather conservative goal. Optimization is

envisioned based on experience with prototypes.

The radial form of the detector does not allow for 90 degrees x-y wires in the chamber. Thus, the wires of each layer are at alternating angle of $\pm$ 10°, called the stereo-angle, from the axis of the drift chamber. We use stereo-angles between wires to determine the coordinate along the beam axis (z). This setting makes it possible to use a very thin forward end-plate to reduce multiple scattering of the outgoing high-energy electrons. A rough estimate of the tension due to about 2600 of 30 cm long wires is under 600 kg, which appears to be reasonable for a composite endplate.

Our drift chamber cells are composed of one sense wire made of gold plated tungsten surrounded by field wires, however the presence of the 5 T magnetic field complicates the field lines. Several cell configurations have been studied with MAGBOLTZ [24] and will be tested in a prototype (see section 2.4). For now, we decided to choose a conservative configuration as shown in Fig. 2.3. The sense wire is surrounded by 6 field wires placed equidistantly from it in a hexagonal pattern. The distance between the sense and field wires is constant and equal to 2 mm. Two adjacent cells share the field wire placed between them. The current design will have 8 layers of cells of increasing radius. The simulation code MAGBOLTZ is calculating the drift speed and drift paths of the electrons (Fig. 2.3). With a moderate electric field, the drift speed is around 10 microns/ns, the average drift time expected is thus 250 ns (over 2 mm). Assuming a conservative 10 ns time resolution, the spatial resolution is expected to be around 200 microns due to field distortions and spread of the signal.

The maximum occupancy, shown in Fig. 2.4, is expected to be of 5% for the inner most wires at 10^{35} cm^{-2}s^{-1} (including the target windows). This is the maximum available luminosity for the baseline CLAS12 and is obtained based on the physics channels depicted in Fig. 2.5, assuming an integration time of 200 ns and considering a readout wire separation of 4 mm. This amount of accidental hits does not appear to be reasonable for a good tracking quality, we therefore decided to run only at half this luminosity for our main production run. This will keep occupancy below 3%, which is a reasonable amount for a drift chamber to maintain high tracking efficiency. When running the coherent processes with the ^{4}He target, it is not necessary to detect the protons[2], and the rate of accidental hits can then be highly reduced by increasing the detection threshold, thus making the chamber blind to protons[3]. In this configuration, considering that our main contribution to occupancy are quasi-elastic protons, we are confident that the ALERT can work properly at 10^{35} cm^{-2}s^{-1}.

We are currently investigating two options to read out the signals from the wires. The first option would be to use the same preamplifier as the one developed for the CLAS inner calorimeter and improved for the Heavy Photon Search [25] experiment installed in Hall B.

[2]This running condition is specific to the proposal "Partonic Structure of Light Nuclei" in the ALERT run group.

[3]The CLAS *eg6* run period was using the RTPC in the same fashion.

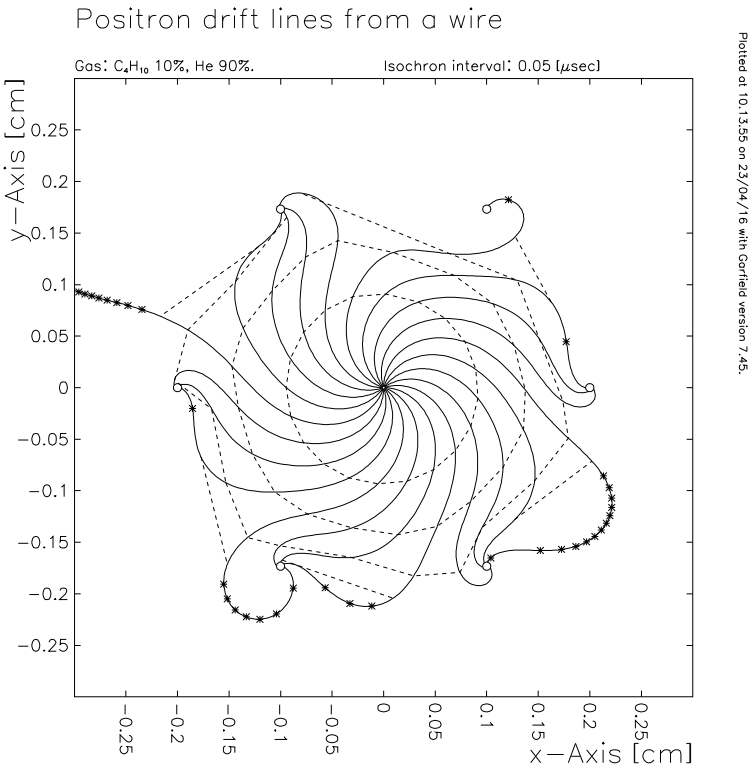

Figure 2.3: Drift lines simulated using MAGBOLTZ [24] for one sense wire (at the center) surrounded by 6 field wires. The two electric field lines leaving the cell disappear when adjusting the voltages on the wires. Dashed lines are isochrones spaced by 50 ns. This shows that the maximum drift time is about 250 ns.

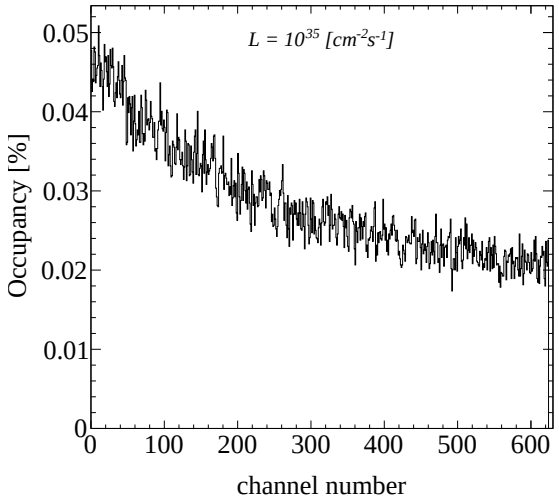

Figure 2.4: A full Geant4 simulation of the ALERT drift chamber hit occupancy at a luminosity of 10^{35} cm^{-2}s^{-1}. The channel numbering starts with the inner most wires and works outwards.

Depending on the gain in the drift chamber and the number of primary ionizations, it is possible to tune the gain of the preamplifier to adapt it to the needs of this experiment. More studies will be needed to evaluate how the gains of the chamber and the preamplifier can be tuned to ensure a noise that allows to select a threshold high enough to be blind to minimum ionizing particles. The time resolution of HPS has been shown to be few-hundred picoseconds for all crystals (Fig. 2.6) which is much better than our requirements.

The second option would be to use the electronics used by the Micromegas of CLAS12, known as the DREAM chip. Its dynamic range and time resolution seem to correspond to the need of our drift chamber. To ensure that it is the case, tests with a prototype will be performed (see section 2.4).

2.2.2 The scintillator array

The scintillator array will serve two main purposes. First, it will provide a useful complementary trigger signal because of its very fast response time, which will reduce the random background triggers. Second, it will provide particle identification, primarily through a time-of-flight measurement, but also by a measurement of the particle total energy deposited and path length in the scintillator which is important for doubly charged ions.

The length of the scintillators cannot exceed roughly 40 cm to keep the time resolution below 150 ps. It must also be segmented to match with tracks reconstructed in the drift chamber. Since ^{3}He and ^{4}He will travel at most a few mm in the scintillator for the highest anticipated momenta ($\sim$ 400 MeV/c), a layered scintillator design provides an extra

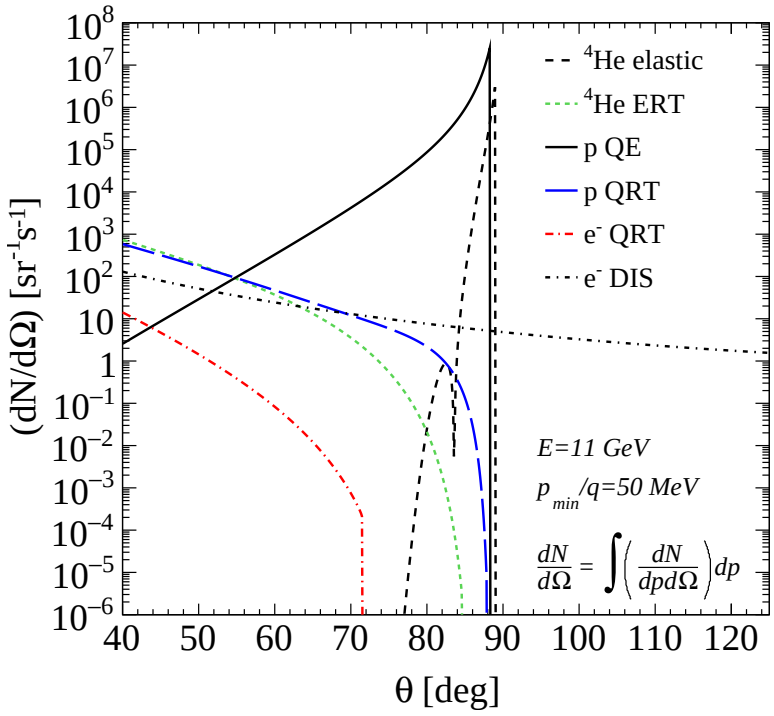

Figure 2.5: The rates for different processes as function of angle. The quasi-elastic radiative tails (QRT), ^{4}He elastic radiative tail (ERT), and DIS contributions have been integrated over momenta starting at $p/q = 50$ MeV/c, where q is the electric charge of the particle detected.

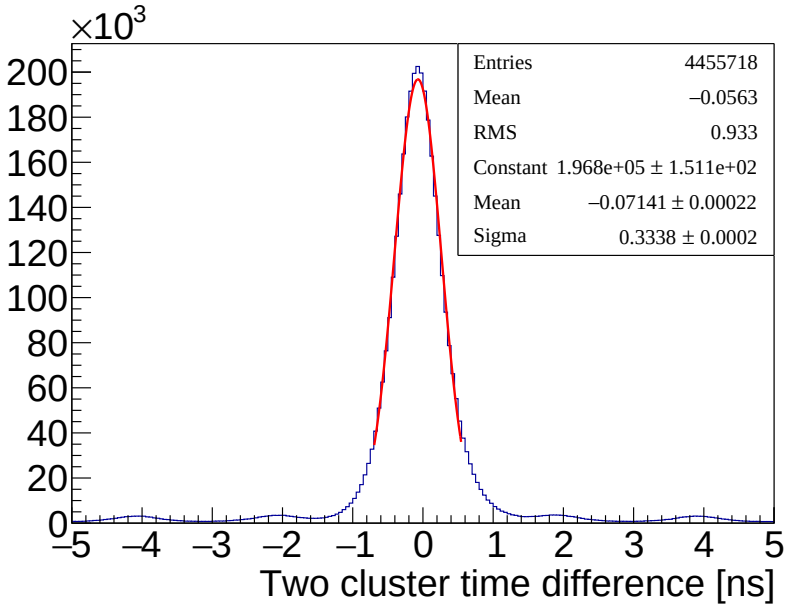

Figure 2.6: Typical time resolution of a crystal for HPS calorimeter.

handle on particle identification by checking if the range exceeded the thickness of the first scintillator layer.

The initial scintillator design consists of a thin (2 mm) inner layer of 60 bars, 30 cm in length, and 600 segmented outer scintillators (10 segments 3 cm long for each inner bar) wrapped around the drift chamber. Each of these thin inner bars has SiPM detectors attached to both ends. A thicker outer layer (18 mm) will be further segmented along the beam axis to provide position information and maintain good time resolution.

For the outer layer, a dual ended bar design and a tile design with embedded wavelength shifting fiber readouts similar to the forward tagger's hodoscope for CLAS12 [26] were considered. After simulating these designs, it was found that the time resolution was insufficient except only for the smallest of tile designs ($15\times15\times7$ mm^3). Instead of using fibers, a SiPM will be mounted directly on the outer layer of a keystone shaped scintillator that is 30 mm in length and 18 mm thick. This design can be seen in Fig. 2.7 which shows a full Geant4 simulation of the drift chamber and scintillators. By directly mounting the SiPMs to the scintillator we collect the maximum signal in the shortest amount of time. With the large number of photons we expect, the time resolution of SiPMs will be a few tens of ps, which is well within our target.

The advantage of a dual ended readout is that the time sum is proportional to the TOF

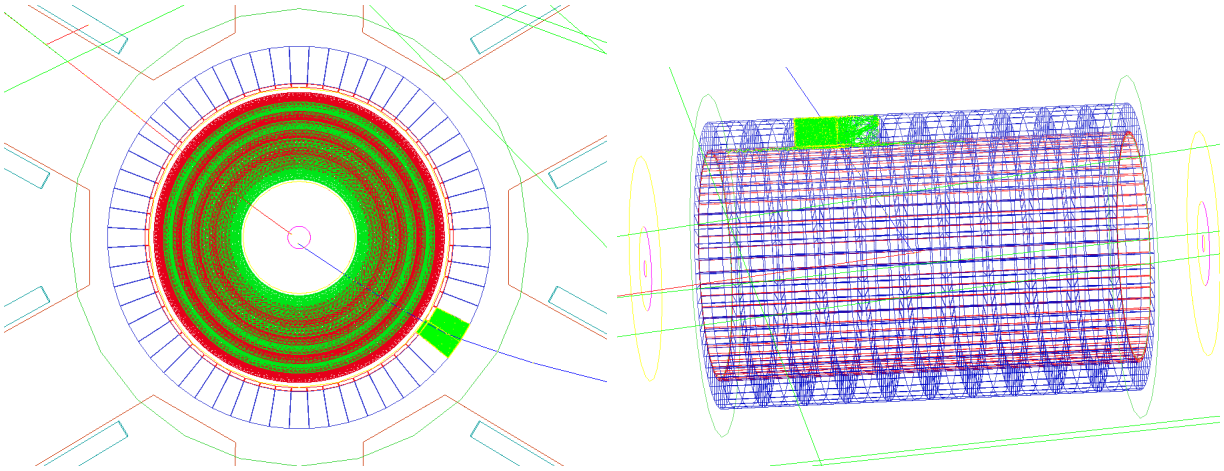

Figure 2.7: Geant4 simulation of a proton passing through the recoil drift chamber and scintillator hodoscope. The view looking downstream (left) shows the drift chamber's eight alternating layers of wires (green and red) surrounded by the two layers of scintillator (red and blue). Simulating a proton through the detector, photons (green) are produced in a few scintillators.

plus a constant. The improved separation of different particles can be seen in Fig. 2.8. Reconstructing the position of a hit along the length of a bar in the first layer is important for the doubly charged ions because they will not penetrate deep enough to reach the second layer of segmented scintillator.

2.3 Reconstruction

The general detection and reconstruction scheme for ALERT is as follows. Fitting a track with the drift chamber and scintillator position information yields a track radius which is proportional to the transverse momentum over the charge. Next, using the scintillator time-of-flight, the particles are separated and identified by their mass-to-charge ratio, therefore leaving a degeneracy for the deuteron and α particles.

The degeneracy between deuteron and α particles can be resolved in a few ways. The first and most simple way is to observe that an α will almost never make it to the second layer and therefore the absence (presence) of a signal would indicate the particle is an α (deuteron). Furthermore, as will be discussed below, the measured dE/dx will differ for ^{4}He and ^{2}H, therefore, taking into account energy loss in track fitting alone can provide separation. Additionally taking further advantage of the measured energy deposited in the scintillators can help separate the αs and deuterons.

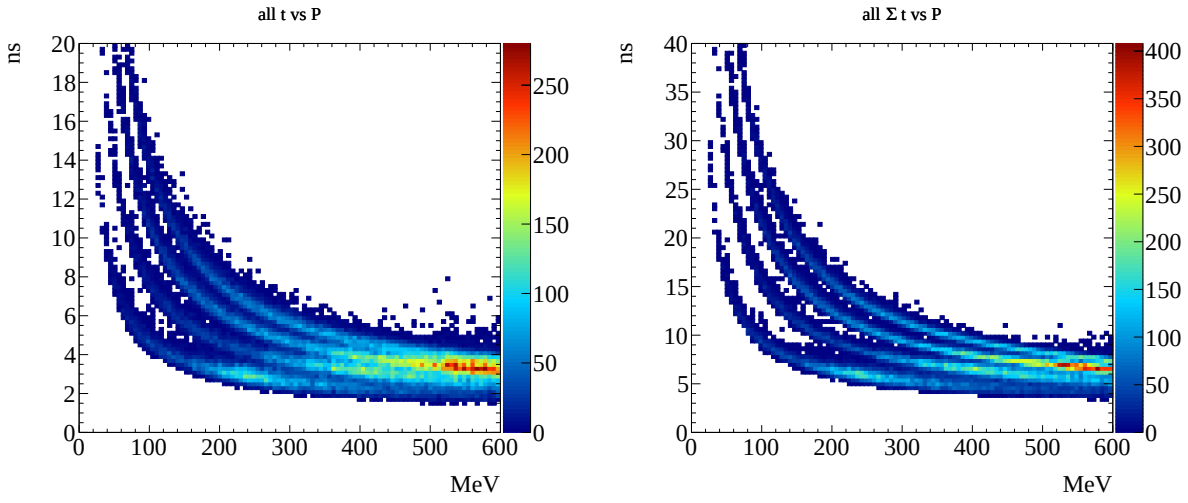

Figure 2.8: Simulated TOF for the various recoil particles vs Momentum. The TOF from just a single readout is shown on the left and the sum of the dual ended readout is shown on the right.

In the studies we present here, we do not include these latter step. However, it is important to point out that extra information is available to us in form of energy deposited in both the drift chamber and the two scintillator layers. In a full (offline) reconstruction these will give extra constraints on the identification but also on the total momentum of the detected nucleus.

As mentioned earlier, we also want a DAQ trigger, that is independent of the CLAS12 triggers. This trigger will be given by the scintillator, in coincidence with signal in a number of layers in the drift chamber. The exact number of drift chamber layers needed for the trigger will be determined during the commissioning based on actual noise and occupancy levels.

2.3.1 Track Fitting

The track obtained from a helix fitter is used to determine the coordinates of the vertex and the transverse momentum of the particle. The energy deposited in the scintillators can also be used to determine the kinetic energy of the nucleus. The feasibility and precision of the proposed vertex reconstruction and particle identification scheme were investigated with GEANT4 simulation.

The simulation of the recoil detector has been implemented with the full geometry and

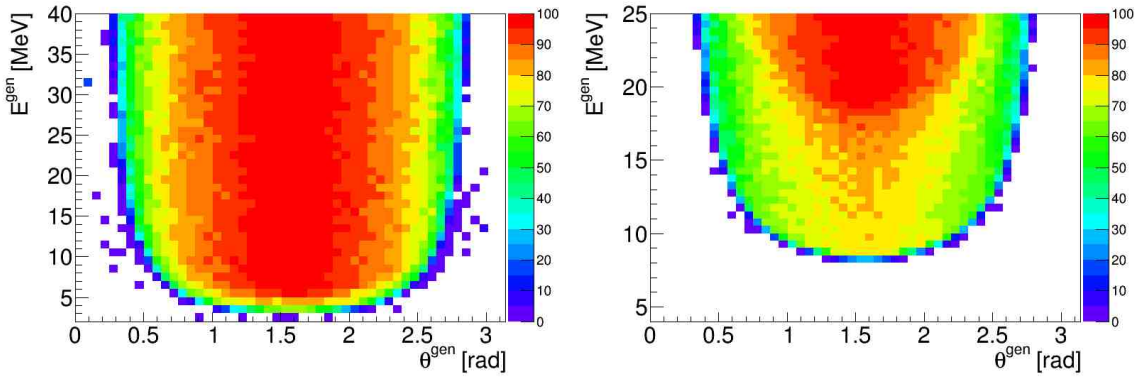

Figure 2.9: Simulated recoil detector acceptance percentage, for protons (left) and ^{4}He (right), when requiring energy deposition in the scintillators arrays.

material specifications. It includes a 5 Tesla homogeneous solenoid field. The entire detector is filled with a very light gas mixture of He(90%) and C_4H_{10}(10%) set at atmospheric pressure to reduce the energy loss and limit the energy deposition by minimum ionizing particles.

2.3.2 Track Reconstruction and Particle Identification

In the current study all recoil species are generated with the same distributions: flat in momentum from threshold up to 40 MeV ($\sim$ 250 MeV/c) for protons and about 25 MeV for other particles; isotropic angular coverage; flat distribution in z-vertex; and a radial vertex coordinate smeared around the beam line center by a Gaussian distribution of sigma equal to the expected beam radius (0.200 mm).

With the requirement that the particle reaches the scintillator and with a 30 cm length limit, there is a smoothly varying acceptance when averaged over the z-vertex position. This is shown from simulation in Fig. 2.9 for the lightest and heaviest recoil nuclei. However, this is a conservative estimate, since it only uses tracking information. A more elaborate PID scheme may be able to accommodate a larger acceptance for lower energy recoils.

First, the tracking capabilities of the recoil detector are investigated assuming a spatial resolutions of 200 μm for the drift chamber. The wires are strung in the z-direction with a stereo angle of 10°. For particles stopped in the scintillators, the resulting difference between generated and reconstructed variables from simulation is shown in Fig. 2.10 for ^{4}He particles. The momentum for protons and ^{4}He was also reconstructed (Fig. 2.11) from the radius of the helix assuming a uniform 5 T field. From these plots, it is clear that the resolutions required are fulfilled.

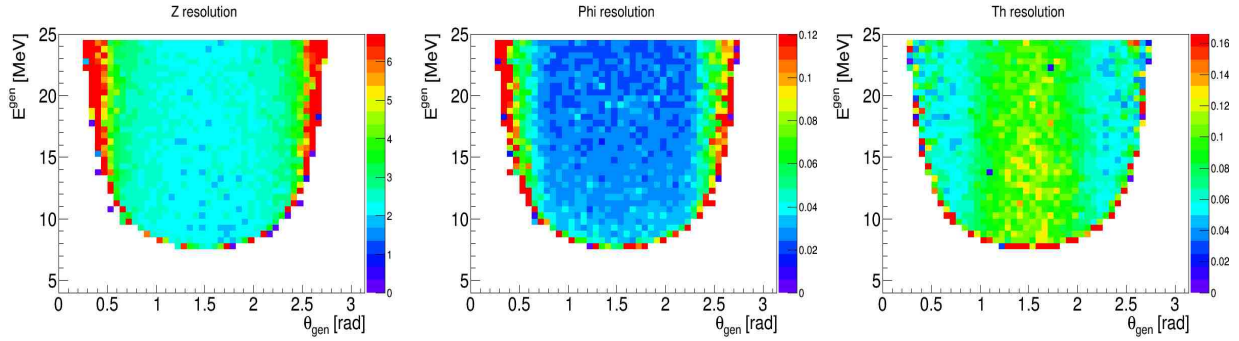

Figure 2.10: Simulated resolutions, integrated over z for ^{4}He, of the z-vertex (in mm) and the polar and azimuthal angles (in rad) for the lowest energy regime when the recoil track reaches the scintillator. Note the z-axis is in units of percent.

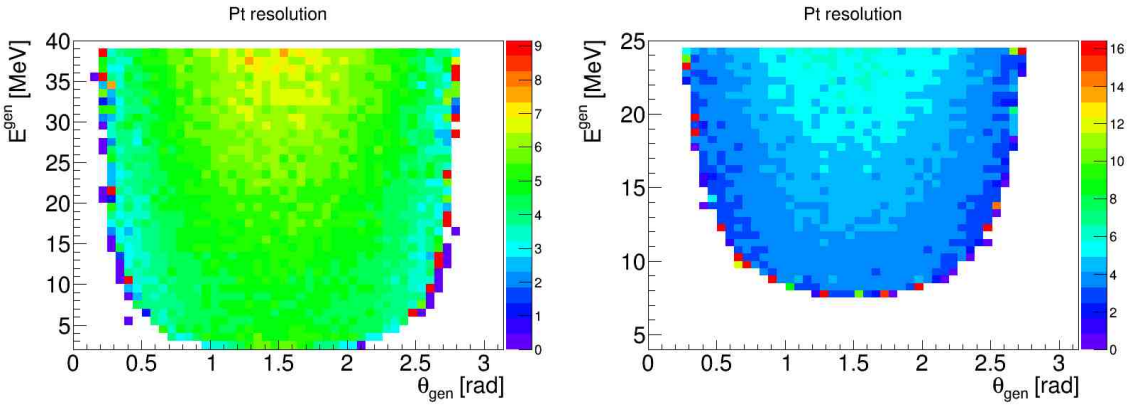

Figure 2.11: Simulated momentum resolutions for proton (left) and ^{4}He (right) integrated over z, when the recoil track reaches the scintillators array. Note the z-axis is in units of percent.

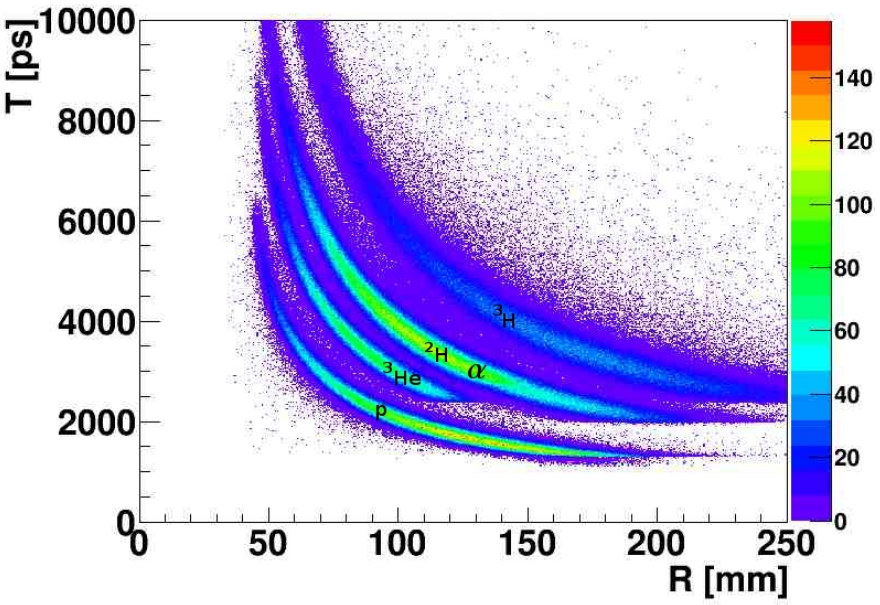

Figure 2.12: Simulated time of flight at the scintillator versus the reconstructed radius in the drift chamber. The bottom band corresponds to proton, next band is the ^{3}He nuclei, ^{2}H and α are overlapping in the third band, the uppermost band is ^{3}H. ^{2}H and α are separated using dE/dx.

Next, the particle identification scheme is investigated. The scintillators have been designed to ensure a 150 ps time resolution. To determine the dE/dx resolution, measurements will be necessary for the scintillators and for the drift chamber as this depends on the detector layout, gas mixture, its electronics, voltages... Nevertheless, from [27], one can assume that with the 8 drift chamber measurements and the measurements in the scintillators, the energy resolution should be around 10% or better.

Under those conditions, a clean separation of three of the five nuclei is shown in Fig. 2.12 which represents the time of arrival in the scintillator as a function of the reconstructed radius in the drift chamber. ^{2}H and α are separated using dE/dx in the drift chamber and in the scintillators.

To quantify the separation power of our device, we simulated an equal quantity of each species. We obtained a particle identification efficiency of 99% for protons, 95% for ^{3}He and 98% for ^{3}H and around 90% for ^{2}H and α with equally excellent rejection factors. It is important to note that for this analysis, only the energy deposited in the scintillators was used, not the energy deposited in the drift chamber nor the path length in the scintillators, thus

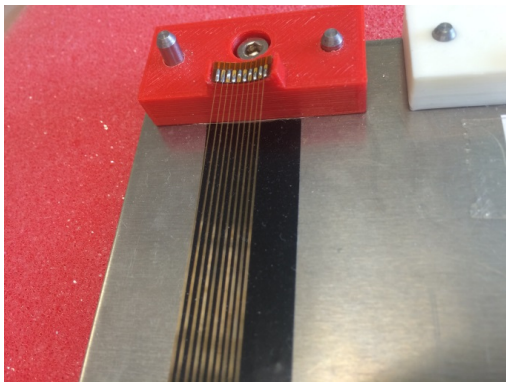

Figure 2.13: Welded wires on a curved structure with a 2 mm gap between each wire.

these number are very conservative. This analysis suggests that the proposed reconstruction and particle identification schemes for this design are quite promising. Studies, using both software and prototyping, are ongoing to determine the optimal detector parameters to minimize the detection threshold while maximizing particle identification efficiency. The resolutions presented above have been implemented in a fast Monte-Carlo used in the next section to evaluate the impact on our measurements.

2.4 Drift chamber prototype

Since the design of the drift chamber presents several challenges, we decided early to start the R&D for the project and build a prototype to investigate the feasibility. This section presents the work done in Orsay to address the main questions concerning the mechanics that needed to be answered:

- Can we build a stereo drift chamber with a 2 mm gap between wires?
- Can we design a frame that can be quickly changed in case of a broken wire?
- Can the forward structure be both light to reduce the multiple scattering and rigid enough to support the tension due to the wires?

For the first question, small plastic structures realized with a 3D printer were tested and wires welded on it, as shown in Fig. 2.13. This demonstrated our ability to weld wires with a 2 mm gap on a curved structure.

To limit issues related to broken wires, we opted for a modular detector made of identical sectors. Each sector covers 20° of the azimuthal angle (Fig. 2.14) and can be rotated around the beam axis to be separated from the other sectors. This rotation is possible due to the absence of one sector, leaving a 20° dead angle. Then, if a wire breaks, its sector can be

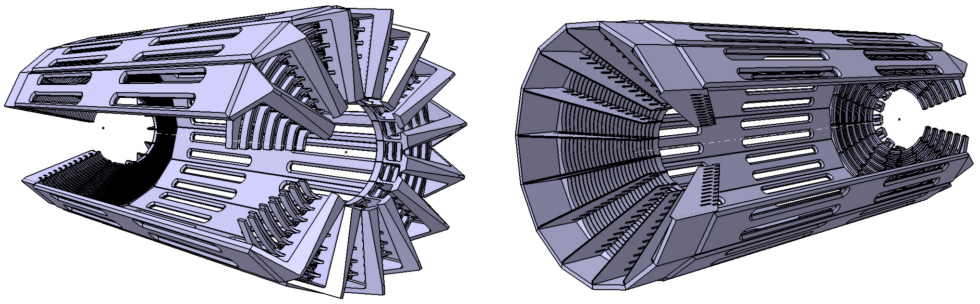

Figure 2.14: Upstream (left) and downstream (right) ends of the prototype detector in CAD with all the sectors included.

removed independently and replaced by a spare. Plastic and metallic prototype sectors were made with 3D printers to test the assembling procedure and we have started the construction of a full size prototype of one sector.

The shape of each sector is constrained by the position of the wires. It has a triangular shape on one side and due to the stereo angle, the other side looks like a pine tree with branches alternatively going left and right from a central trunk (Fig. 2.15).

The last question about the material used to build the structure will be studied in details with future prototypes. Nevertheless, current design plans are to use carbon in place of the aluminum in the forward region and titanium for the backward structure. The prototype was designed to check the mechanical requirements summarized above but also to verify the different cell configurations, and to test the DREAM electronics (time resolution, active range, noise). Since a total of five sectors have been build for tests, this will allow us to check that the elements can be properly positioned relatively to each other and one sector will be completely equipped with wires to be tested with a cosmic test bench and an α source.

2.5 Other options for a Low Energy Recoil Detector

We explored other available solutions for the low-energy recoil tracker (ALERT) with adequate momentum and spatial resolution, and good particle identification for recoiling light nuclei (p, ^{3}H and ^{3}He). After investigating the feasibility of the proposed measurements using the CLAS12 Central Detector and the BoNuS Detector [28, 29], we concluded that we needed to build a dedicated detector. We summarize in the following the facts that led us to this conclusion.

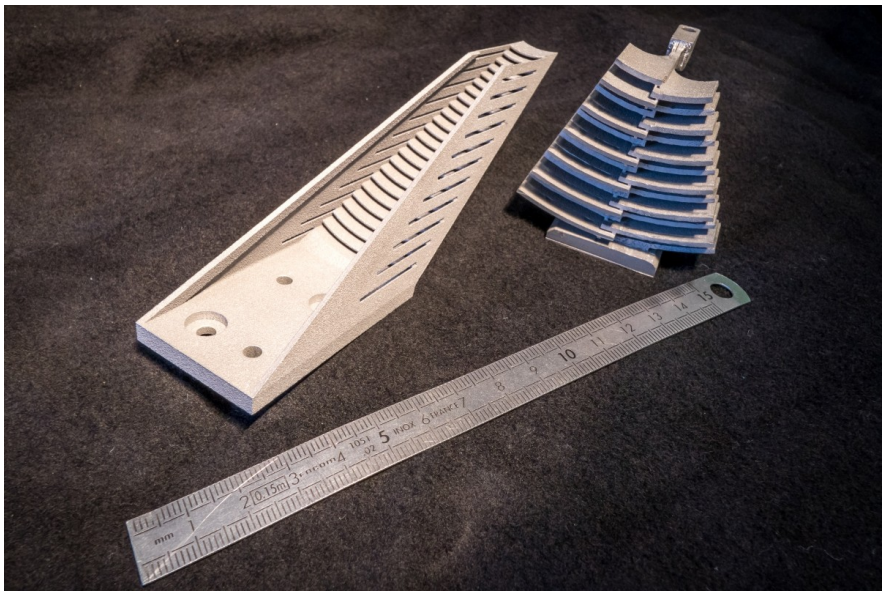

Figure 2.15: Mechanics of one sector for the prototype made with 3D printer.

2.5.1 Central Detector

The CLAS12 Central Detector [20] is designed to detect various charged particles over a wide momentum and angular range. The main detector package includes:

- Solenoid Magnet: provides a central longitudinal magnetic field up to 5 Tesla, serves to curl emitted low energy Møller electrons and determine particle momenta through tracking.
- Central Tracker: consists of 3 layers of silicon strips and 3 layers of Micromegas. The thickness of a single silicon layer is 300μm.
- Central Time-of-Flight: an array of scintillator paddles with a cylindrical geometry of radius 26 cm and length 50 cm; the thickness of the detector is 2 cm with designed timing resolution of $\sigma_t = 50$ ps, used to separate pions and protons up to 1.2 GeV/c.

The current design, however, is not optimal for low energy particles ($p < 300$ MeV/c) due to the energy loss in the first 2 silicon strip layers. The momentum detection threshold is ~ 200 MeV/c for protons, ~ 350 MeV/c for deuterons and even higher for ^{3}H and ^{3}He. These values are significantly too large for our proposed measurements, which makes the CLAS12 central detector not suitable for our measurements.

Detectors	RTPC	New Tracker
Drift region radius	4 cm	5 cm
Longitudinal length	$\sim$ 40 cm	$\sim$ 40 cm
Gas mixture	80% helium/20% DME	90% helium/10% isobutane
Azimuthal coverage	360°	340°
Momentum range	70-250 MeV/c protons	70-250 MeV/c protons
Transverse mom. resolution	10% for 100 MeV/c protons	10% for 100 MeV/c protons
z resolution	3 mm	3 mm
Solenoidal field	$\sim$ 5 T	$\sim$ 5 T
ID all light nuclei	No	Yes
Trigger	can not be included	can be included

Table 2.2: Comparison between the RTPC (left column) and the new tracker (right column).

2.5.2 BoNuS12 Radial Time Projection Chamber

The original BoNuS detector was built for Hall B experiment E03-012 to study neutron structure at high x_B by scattering electrons off an almost on-shell neutron inside deuteron. The purpose of the detector was to tag the low energy recoil protons ($p > 60$ MeV/c). The key component for detecting the slow protons was the Radial Time Projection Chamber (RTPC) based on Gas Electron Multipliers (GEM). A later run period (eg6) used a ^{4}He gas target and a newly built and improved RTPC to detect recoiling α particles in coherent DVCS scattering. The major improvements of the eg6 RTPC were full cylindrical coverage and a higher data taking rate.

The approved 12 GeV BoNuS (BoNuS12) proposal is planning to use a similar device with some upgrades. The target gas cell length will be doubled, and the new RTPC will be longer as well, leading to a doubling in luminosity and an increased acceptance. Taking advantage of the larger bore ($\sim$ 700 mm) of the 5 Tesla solenoid magnet, the maximum radial drift length will be increased from the present 3 cm to 4 cm, improving the momentum resolution by 50% [29] and extending the momentum coverage. The main features of the proposed BoNuS12 detector are summarized in Table 2.2.

In principle, particle identification can be obtained from the RTPC through the energy loss dE/dx in the detector as a function of the particle momentum (see Fig. 2.16). However, with such a small difference between ^{3}H and ^{3}He, it is nearly impossible to discriminate between them on an event by event basis because of the intrinsic width of the dE/dx distributions. This feature is not problematic when using deuterium target, but makes the RTPC no longer a viable option for our tagged EMC and tagged DVCS measurements which require a ^{4}He target and the detection of ^{4}He, ^{3}He, ^{3}H, deuterons and protons.

Another issue with the RTPC is its slow response time due to the long drift time

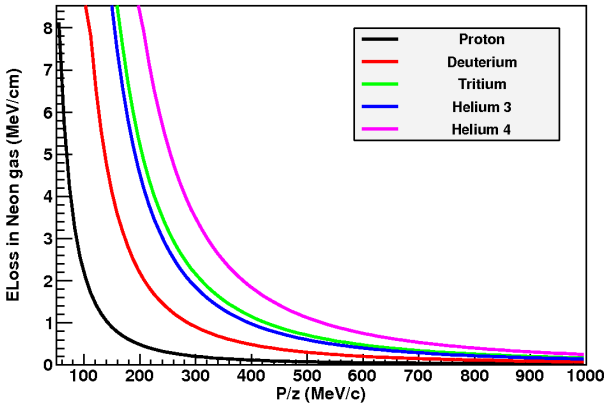

Figure 2.16: Calculation of energy loss in Neon gas as a function of the particle momentum divided by its charge for different nuclei.

($\sim 5\mu$s). If a fast recoil detector could be included in the trigger it would have a significant impact on the background rejection. Indeed, in about 90% DIS on deuteron or helium the spectator fragments have too low energy or too small angle with the beam line to get out of the target to be detected. Since the data acquisition speed was the main limiting factor for both BoNuS and eg6 runs in CLAS, including the recoil detector in the trigger would allow us to run at higher luminosities. Indeed events without a hit in the recoil detector would not be recorded and this will significantly reduce the trigger's frequency.

2.5.3 Summary

As explained in the previous sections, the threshold of the CLAS12 inner tracker is clearly too high to be used for our measurements. On the other hand, the recoil detector planned for BoNuS12, a RTPC, is not suitable due to its inability to distinguish all kind of particles we need to measure. Moreover, as the RTPC cannot be efficiently included in the trigger, a lot of background events are sent to the readout electronics, which will cause its saturation and limit the maximum luminosity the detector can handle. Therefore, we propose to use A Low Energy Recoil Tracker (ALERT) based on a new detector design, described in the previous sections, that would provide good timing and energy loss information and a total energy measurement for each track. The fast timing will allow a tight time coincidence with CLAS12, thereby reducing the background that was encountered in previous RTPC detectors. The recoil detector can be included in the data acquisition trigger, which will significantly reduce triggering on events from the target windows, which are outside the acceptance and events with recoil too slow to exit the target.

Finally, the use of time of flight and dE/dx measurements will provide improved particle

identification for the recoiling nuclei without ambiguity for ^{3}H and ^{3}He identification. The features and requirements for this new detector are compared with the current RTPC design for BoNuS12 in Table 2.2. The transverse momentum and z resolution are chosen following the BoNuS specifications.

2.6 Technical contributions from the research groups

This effort is led by four research groups, Argonne National Lab (ANL), Institut de Physique Nucléaire d'Orsay (IPNO), Jefferson Lab and Temple University (TU).

Jefferson Lab is the host institution. ANL, IPNO and TU have all contributed technically to CLAS12. ANL was involved in the construction of the high-threshold Cherenkov counters (HTCC) for CLAS12. ANL has a memorandum of understanding (MOU) with JLab on taking responsibility for the HTCC light collection system including testing the photomultipliers and the magnetic shielding. For the RICH detector for CLAS12, ANL developed full GEANT-4 simulations in addition to the tracking software. ANL also developed the mechanical design of the detector support elements and entrance and exit windows in addition to the front-end electronics cooling system. IPNO took full responsibility for the design and construction of CLAS12 neutron detector (CND). The CND was successfully delivered to Jefferson Lab. TU played an important role in the refurbishment of the low threshold Cherenkov counters (LTCC), which was completed recently. All 216 photomultipliers have been coated with wavelength shifting material (p-Terphenyl) at Temple University, which resulted in a significant increase in the number of photoelectrons response.

The three institutions have already shown strong technical commitment to JLab 12 GeV upgrade, with a focus on CLAS12 and this proposal is a continuation of that commitment.

2.6.1 Argonne National Laboratory and Temple University

The ANL medium energy group is responsible for the ALERT scintillator system, including scintillation material, light collection device and electronics. First results of simulations have led to the design proposed here. This work will continue to integrate the scintillator system with the wire chamber. ANL will collaborate closely with Temple University to test the light detection system. Both institutions will be responsible to assemble and test the detector.

2.6.2 Institut de Physique Nucléaire d'Orsay

The Institut de Physique Nucléaire d'Orsay is responsible for the wire chamber and the mechanical structure of the detector design and construction. As shown in the proposal, this work has already started as part of a wider R&D program focused on nuclear fragments

detection with light wire chambers. A first prototype is being built to test different cell forms, wire material, wire thickness, pressure, etc. This experience will lead to a complete design of the ALERT detector integrating the scintillator built at ANL, the gas distribution system and the electronic connections. The funding already secured for this program should allow for the construction of these mechanical parts and the wire chamber itself.

Funding is also available, in partnership with *CEA Saclay*, to test the use of the DREAM front-end chip for our wire chamber. Further tests are planned to adapt the electronics to the ALERT chamber or test other chips. This chip will be used for the CLAS Micromegas, so we expect its integration to be straightforward when the ALERT run group will need it.

2.6.3 Jefferson Laboratory

We expect Jefferson Laboratory to help with the settings of the beam line. In particular, the maximum beam current will be around 500 nA for the run at 10^{35} cm^{-2}s^{-1}, which is not common for Hall-B. We also expect JLab to design and build the target for the experiment as it will be a very similar target as the ones build for CLAS Bonus and eg6 run.

We also expect Jefferson Laboratory to provide assistance in the detector installation in the Hall and to connect the electronics of ALERT to the acquisition and trigger systems of CLAS12 in addition to slow controls.

Summary and Beam Time Request

In summary, there is a broad experimental program to be carried out using CLAS12 and ALERT detectors. This fourth proposal only shows a flavor of the endless possibilities. The ALERT collaboration has every intention of mining the data that will be collected during the ALERT run and advance our understanding of nuclear QCD. This proposal focuses on exclusive π^0 production off ^{4}He, coherent exclusive DVCS off deuteron and DVCS in three-body break up reactions. These topics are closely connected to the ones proposed in the three proposals which compose the ALERT run group. There is no additional beam time request. These three measurements are perfectly compatible with the running conditions of the ALERT run group.

Appendix A

Twist-3 electroproduction cross-section off a spinless target

The differential cross section for real photon electroproduction of a longitudinally-polarized electron beam on a spin-zero target can be expressed as [30]:

$$\frac{d^5\sigma_\lambda}{dx_A dQ^2 dt d\phi_e d\phi} = \frac{\alpha^3}{16\pi^2}\frac{x_A\, y^2}{Q^4\sqrt{1+\varepsilon^2}}\frac{|\mathcal{T}_{BH}|^2 + |\mathcal{T}^\lambda_{DVCS}|^2 + \mathcal{I}^\lambda_{BH*DVCS}}{e^6} \tag{A.1}$$

where $y = \frac{p\cdot q}{p\cdot k}$, $\varepsilon = \frac{2x_A M_A}{Q}$ and $x_A = \frac{Q^2}{2p\cdot q}$. The different amplitudes can be written as:

$$|\mathcal{T}_{BH}|^2 = \frac{e^6(1+\varepsilon^2)^{-2}}{x_A^2 y^2 t \mathcal{P}_1(\phi)\mathcal{P}_2(\phi)}\sum_{n=0}^{2} c_n^{BH}\cos(n\phi) \tag{A.2}$$

$$|\mathcal{T}_{DVCS}|^2 = \frac{e^6}{y^2Q^2}\sum_{n=0}^{2}\left(c_n^{DVCS}\cos(n\phi) + \lambda s_n^{DVCS}\sin(n\phi)\right) \tag{A.3}$$

$$\mathcal{I}_{BH*DVCS} = \frac{\pm e^6}{x_A y^3 t\,\mathcal{P}_1(\phi)\mathcal{P}_2(\phi)}\sum_{n=0}^{3}\left(c_n^{I}\cos(n\phi) + \lambda s_n^{I}\sin(n\phi)\right) \tag{A.4}$$

The beam-spin asymmetry (A_{LU}) with the two opposite helicities of a longitudinally-polarized electron beam (L) on a spin-zero target (U) can be written as:

$$A_{LU} = \frac{D_1\sum_{n=1}^{2} s_n^{DVCS}\sin(n\phi) + D_2\sum_{n=1}^{3} s_n^{I}\sin(n\phi)}{\sum_{n=0}^{n=2} c_n^{BH}\cos(n\phi) + D_1\sum_{n=0}^{n=2} c_n^{DVCS}\cos(n\phi) + D_2\sum_{n=0}^{n=3} c_n^{I}\cos(n\phi)} \tag{A.5}$$

with the kinematical variables $D_1 = \frac{x_A^2 t(1+\varepsilon^2)^2}{Q^2}P_1(\phi)P_2(\phi)$ and $D_2 = \frac{x_A(1+\varepsilon^2)^2}{y}$.
The Bethe-Heitler Fourier coefficients of a spin-0 target are defined Appendix **??**.

At twist-3, the $|\mathcal{T}_{DVCS}|^2$ writes as a function of the following Fourier coefficients

$$c_0^{\rm DVCS} = 2\frac{2-2y+y^2+\frac{\varepsilon^2}{2}y^2}{1+\varepsilon^2}\mathcal{C}^{\rm DVCS}(\mathcal{H},\mathcal{H}^*;\mathcal{H}_T,\mathcal{H}_T^*)+\frac{16K^2\mathcal{H}_{\rm eff}\mathcal{H}_{\rm eff}^*}{(2-x_B)^2(1+\varepsilon^2)}\,, \tag{A.6}$$

$$\left\{\begin{array}{c} c_1^{\rm DVCS} \\ s_1^{\rm DVCS}\end{array}\right\} = \frac{8K}{(2-x_B)(1+\varepsilon^2)}\left\{\begin{array}{c} (2-y)\,\Re{\rm e} \\ -\lambda y\sqrt{1+\varepsilon^2}\,\Im{\rm m}\end{array}\right\}\mathcal{C}^{\rm DVCS}\left(\mathcal{H}^{\rm eff};\mathcal{H}^*;\mathcal{H}_T^*\right)\,, \tag{A.7}$$

$$c_2^{\rm DVCS} = \frac{16\mathcal{Q}^2K^2}{M^2(2-x_B)^2(1+\varepsilon^2)}\Re{\rm e}\,\mathcal{C}_T^{\rm DVCS}\left(\mathcal{H},\mathcal{H}_T^*\right)\,. \tag{A.8}$$

where the bilinear CFFs and the effective twist-three CFF $\mathcal{H}_3^{\rm eff}$ read:

$$\begin{aligned}\mathcal{C}^{\rm DVCS}\left(\mathcal{H},\mathcal{H}^*,\mathcal{H}_T,\mathcal{H}_T^*\right) &= \mathcal{H}\mathcal{H}^*+\frac{\widetilde{K}^4}{(2-x_B)^4}\mathcal{H}_T\mathcal{H}_T^*\,,\\ \mathcal{C}^{\rm DVCS}\left(\mathcal{H}_{\rm eff};\mathcal{H}^*;\mathcal{H}_T^*\right) &= \mathcal{H}_{\rm eff}\left(\mathcal{H}^*+\frac{2\widetilde{K}^2}{M^2(2-x_B)^2}\mathcal{H}_T^*\right)\\ \mathcal{C}_T^{\rm DVCS}\left(\mathcal{H},\mathcal{H}_T^*\right) &= \mathcal{H}\mathcal{H}_T^*\,.\end{aligned} \tag{A.9}$$

$$\mathcal{H}^{\rm eff} \equiv -2\xi\left(\frac{1}{1+\xi}\mathcal{H}+\mathcal{H}_+^3-\mathcal{H}_-^3\right)\,, \tag{A.10}$$

with the CFFs $\mathcal{H}_\pm^3$ related to functions $H_\pm^3$ given by a convolution of the twist-two GPD H and the so-called Wandzura-Wilczek kernel provided one neglects dynamical quark-gluon-quark correlation functions.

The interference amplitude coefficients are written as:

$$c_n^{\mathcal{I}} = C_{++}(n)\,\Re{\rm e}\,\mathcal{C}^{\mathcal{I}}\left(\mathcal{H}\right)+\frac{\sqrt{2}}{2-x_B}\,\frac{\widetilde{K}}{Q}\,C_{0+}(n)\,\Re{\rm e}\,\mathcal{C}^{\mathcal{I}}\left(\mathcal{H}_3^{\rm eff}\right)+\frac{2}{(2-x_B)^2}\,\frac{\widetilde{K}^2}{M^2}\,C_{-+}(n)\,\Re{\rm e}\,\mathcal{C}^{\mathcal{I}}\left(\mathcal{H}_T\right)\,, \tag{A.11}$$

$$s_n^{\mathcal{I}} = S_{++}(n)\,\Im{\rm m}\,\mathcal{C}^{\mathcal{I}}\left(\mathcal{H}\right)+\frac{\sqrt{2}}{2-x_B}\,\frac{\widetilde{K}}{Q}\,S_{0+}(n)\,\Im{\rm m}\,\mathcal{C}^{\mathcal{I}}\left(\mathcal{H}_3^{\rm eff}\right)+\frac{2}{(2-x_B)^2}\,\frac{\widetilde{K}^2}{M^2}\,S_{-+}(n)\,\Im{\rm m}\,\mathcal{C}^{\mathcal{I}}\left(\mathcal{H}_T\right)\,, \tag{A.12}$$

with the CFF components

$$\mathcal{C}^{\mathcal{I}}(\mathcal{H}) = F\mathcal{H}\,,\qquad \mathcal{C}_T^{\mathcal{I}} = F\mathcal{H}_T\,. \tag{A.13}$$

The individual Fourier harmonics are detailed in the following sections.

The explicit expressions for the Fourier coefficients entering the leptonic part of the interference

term are presented herein. For the transverse-transverse harmonics we have

$$
\begin{aligned}
C_{++}(n=0) &= -\frac{4(2-y)\left(1+\sqrt{1+\varepsilon^2}\right)}{(1+\varepsilon^2)^2}\left\{\frac{\widetilde{K}^2}{Q^2}\frac{(2-y)^2}{\sqrt{1+\varepsilon^2}}\right. \\
&\left. +\ \frac{t}{Q^2}\left(1-y-\frac{\varepsilon^2}{4}y^2\right)(2-x_B)\left(1+\frac{2x_B\left(2-x_B+\frac{\sqrt{1+\varepsilon^2}-1}{2}+\frac{\varepsilon^2}{2x_B}\right)\frac{t}{Q^2}+\varepsilon^2}{(2-x_B)(1+\sqrt{1+\varepsilon^2})}\right)\right\}, \\
C_{++}(n=1) &= \frac{-16K\left(1-y-\frac{\varepsilon^2}{4}y^2\right)}{(1+\varepsilon^2)^{5/2}}\left\{\left(1+(1-x_B)\frac{\sqrt{\varepsilon^2+1}-1}{2x_B}+\frac{\varepsilon^2}{4x_B}\right)\frac{x_Bt}{Q^2}-\frac{3\varepsilon^2}{4}\right\} \\
&\quad -4K\left(2-2y+y^2+\frac{\varepsilon^2}{2}y^2\right)\frac{1+\sqrt{1+\varepsilon^2}-\varepsilon^2}{(1+\varepsilon^2)^{5/2}}\left\{1-(1-3x_B)\frac{t}{Q^2}\right. \\
&\qquad\qquad \left. +\frac{1-\sqrt{1+\varepsilon^2}+3\varepsilon^2}{1+\sqrt{1+\varepsilon^2}-\varepsilon^2}\frac{x_Bt}{Q^2}\right\}, \\
C_{++}(n=2) &= \frac{8(2-y)\left(1-y-\frac{\varepsilon^2}{4}y^2\right)}{(1+\varepsilon^2)^2}\left\{\frac{2\varepsilon^2}{1+\varepsilon^2+\sqrt{1+\varepsilon^2}}\frac{\widetilde{K}^2}{Q^2}\right. \\
&\qquad\qquad \left. +\frac{x_Bt\,t'}{Q^4}\left(1-x_B-\frac{\sqrt{1+\varepsilon^2}-1}{2}+\frac{\varepsilon^2}{2x_B}\right)\right\}, \\
C_{++}(n=3) &= -8K\left(1-y-\frac{\varepsilon^2}{4}y^2\right)\frac{\sqrt{1+\varepsilon^2}-1}{(1+\varepsilon^2)^{5/2}}\left\{(1-x_B)\frac{t}{Q^2}+\frac{\sqrt{1+\varepsilon^2}-1}{2}\left(1+\frac{t}{Q^2}\right)\right\}, \\
S_{++}(n=1) &= -\frac{8K(2-y)y}{1+\varepsilon^2}\left\{1+\frac{1-x_B+\frac{\sqrt{1+\varepsilon^2}-1}{2}}{1+\varepsilon^2}\frac{t'}{Q^2}\right\}, \\
S_{++}(n=2) & \\
&= \frac{4\left(1-y-\frac{\varepsilon^2}{4}y^2\right)y}{(1+\varepsilon^2)^{3/2}}\left(1+\sqrt{1+\varepsilon^2}-2x_B\right)\frac{t'}{Q^2}\left\{\frac{\varepsilon^2-x_B(\sqrt{1+\varepsilon^2}-1)}{1+\sqrt{\varepsilon^2+1}-2x_B}-\frac{2x_B+\varepsilon^2}{2\sqrt{1+\varepsilon^2}}\frac{t'}{Q^2}\right\},
\end{aligned}
\tag{A.14}
$$

while the longitudinal-transverse ones,

$$C_{0+}(n=0) = \frac{12\sqrt{2}K(2-y)\sqrt{1-y-\frac{\varepsilon^2}{4}y^2}}{(1+\varepsilon^2)^{5/2}}\left\{\varepsilon^2 + \frac{2-6x_B-\varepsilon^2}{3}\frac{t}{Q^2}\right\}, \tag{A.15}$$

$$C_{0+}(n=1) = \frac{8\sqrt{2}\sqrt{1-y-\frac{\varepsilon^2}{4}y^2}}{(1+\varepsilon^2)^2}\left\{(2-y)^2\frac{t'}{Q^2}\left(1-x_B+\frac{(1-x_B)x_B+\frac{\varepsilon^2}{4}}{\sqrt{1+\varepsilon^2}}\frac{t'}{Q^2}\right)\right.$$
$$\left. +\frac{1-y-\frac{\varepsilon^2}{4}y^2}{\sqrt{1+\varepsilon^2}}\left(1-(1-2x_B)\frac{t}{Q^2}\right)\left(\varepsilon^2-2\left(1+\frac{\varepsilon^2}{2x_B}\right)\frac{x_Bt}{Q^2}\right)\right\},$$

$$C_{0+}(n=2) = -\frac{8\sqrt{2}K(2-y)\sqrt{1-y-\frac{\varepsilon^2}{4}y^2}}{(1+\varepsilon^2)^{5/2}}\left(1+\frac{\varepsilon^2}{2}\right)\left\{1+\frac{1+\frac{\varepsilon^2}{2x_B}}{1+\frac{\varepsilon^2}{2}}\frac{x_Bt}{Q^2}\right\},$$

$$S_{0+}(n=1) = -\frac{8\sqrt{2}(2-y)y\sqrt{1-y-\frac{\varepsilon^2}{4}y^2}}{(1+\varepsilon^2)^2}\frac{\widetilde{K}^2}{Q^2},$$

$$S_{0+}(n=2) = -\frac{8\sqrt{2}Ky\sqrt{1-y-\frac{\varepsilon^2}{4}y^2}}{(1+\varepsilon^2)^2}\left(1+\frac{\varepsilon^2}{2}\right)\left\{1+\frac{1+\frac{\varepsilon^2}{2x_B}}{1+\frac{\varepsilon^2}{2}}\frac{x_Bt}{Q^2}\right\}.$$

Finally, the helicity-flip transverse-transverse coefficients are

$$
\begin{aligned}
C_{-+}(n=0) &= \frac{8(2-y)}{(1+\varepsilon^2)^{3/2}}\Bigg\{(2-y)^2\frac{\sqrt{1+\varepsilon^2}-1}{2(1+\varepsilon^2)}\frac{\widetilde{K}^2}{Q^2} \\
&\quad + \frac{1-y-\frac{\varepsilon^2}{4}y^2}{\sqrt{1+\varepsilon^2}}\left(1-x_B-\frac{\sqrt{1+\varepsilon^2}-1}{2}+\frac{\varepsilon^2}{2x_B}\right)\frac{x_B t\, t'}{Q^4}\Bigg\}, \\
C_{-+}(n=1) &= \frac{8K}{(1+\varepsilon^2)^{3/2}}\Bigg\{(2-y)^2\frac{2-\sqrt{1+\varepsilon^2}}{1+\varepsilon^2}\left(\frac{\sqrt{1+\varepsilon^2}-1+\varepsilon^2}{2\left(2-\sqrt{1+\varepsilon^2}\right)}\left(1-\frac{t}{Q^2}\right)-\frac{x_B t}{Q^2}\right) \\
&\quad + 2\frac{1-y-\frac{\varepsilon^2}{4}y^2}{\sqrt{1+\varepsilon^2}}\left(\frac{1-\sqrt{1+\varepsilon^2}+\frac{\varepsilon^2}{2}}{2\sqrt{1+\varepsilon^2}}+\frac{t}{Q^2}\left(1-\frac{3x_B}{2}+\frac{x_B+\frac{\varepsilon^2}{2}}{2\sqrt{1+\varepsilon^2}}\right)\right)\Bigg\}, \\
C_{-+}(n=2) &= 4(2-y)\left(1-y-\frac{\varepsilon^2}{4}y^2\right)\frac{1+\sqrt{1+\varepsilon^2}}{(1+\varepsilon^2)^{5/2}}\Bigg\{(2-3x_B)\frac{t}{Q^2} \\
&\quad + \left(1-2x_B+\frac{2(1-x_B)}{1+\sqrt{1+\varepsilon^2}}\right)\frac{x_B t^2}{Q^4}+\left(1+\frac{\sqrt{1+\varepsilon^2}+x_B+(1-x_B)\frac{t}{Q^2}}{1+\sqrt{1+\varepsilon^2}}\frac{t}{Q^2}\right)\varepsilon^2\Bigg\}, \\
C_{-+}(n=3) &= -8K\left(1-y-\frac{\varepsilon^2}{4}y^2\right)\frac{1+\sqrt{1+\varepsilon^2}+\frac{\varepsilon^2}{2}}{(1+\varepsilon^2)^{5/2}}\left\{1+\frac{1+\sqrt{1+\varepsilon^2}+\frac{\varepsilon^2}{2x_B}}{1+\sqrt{1+\varepsilon^2}+\frac{\varepsilon^2}{2}}\frac{x_B t}{Q^2}\right\}, \\
S_{-+}(n=1) &= -\frac{4K(2-y)y}{(1+\varepsilon^2)^2}\left\{1-\sqrt{1+\varepsilon^2}+2\varepsilon^2-2\left(1+\frac{\sqrt{1+\varepsilon^2}-1}{2x_B}\right)\frac{x_B t}{Q^2}\right\}, \\
S_{-+}(n=2) &= -2y\left(1-y-\frac{\varepsilon^2}{4}y^2\right)\frac{1+\sqrt{1+\varepsilon^2}}{(1+\varepsilon^2)^2}\left(\varepsilon^2-2\left(1+\frac{\varepsilon^2}{2x_B}\right)\frac{x_B t}{Q^2}\right) \\
&\quad \times\left\{1+\frac{\sqrt{1+\varepsilon^2}-1+2x_B}{1+\sqrt{1+\varepsilon^2}}\frac{t}{Q^2}\right\}.
\end{aligned}
\tag{A.16}
$$

Bibliography

[1] K. Hafidi *et al.*, "Nuclear Exclusive and Semi-inclusive Physics with a New CLAS12 Low Energy Recoil Detector (LOI-10-009)," *A Letter of Intent to PAC 35*, 2010.

[2] X. Ji, X. Xiong, and F. Yuan, "Transverse Polarization of the Nucleon in Parton Picture," *Phys. Lett.*, vol. B717, pp. 214–218, 2012.

[3] M. Diehl, "Generalized parton distributions with helicity flip," *Eur. Phys. J.*, vol. C19, pp. 485–492, 2001.

[4] S. Ahmad, G. R. Goldstein, and S. Liuti, "Nucleon Tensor Charge from Exclusive pi**o Electroproduction," *Phys. Rev.*, vol. D79, p. 054014, 2009.

[5] S. V. Goloskokov and P. Kroll, "Transversity in hard exclusive electroproduction of pseudoscalar mesons," *Eur. Phys. J.*, vol. A47, p. 112, 2011.

[6] G. R. Goldstein, J. O. G. Hernandez, and S. Liuti, "Easy as π^o: On the Interpretation of Recent Electroproduction Results," *J. Phys.*, vol. G39, p. 115001, 2012.

[7] G. R. Goldstein, J. O. G. Hernandez, and S. Liuti, "Flexible Parametrization of Generalized Parton Distributions: The Chiral-Odd Sector," *Phys. Rev.*, vol. D91, no. 11, p. 114013, 2015.

[8] P. Kroll, "Hard exclusive pion leptoproduction," 2016.

[9] R. Boussarie, B. Pire, L. Szymanowski, and S. Wallon, "Revealing transversity GPDs through the photoproduction of a photon and a ρ meson," *EPJ Web Conf.*, vol. 112, p. 01006, 2016.

[10] I. Bedlinskiy *et al.*, "Exclusive π^0 electroproduction at $W > 2$ GeV with CLAS," *Phys. Rev.*, vol. C90, no. 2, p. 025205, 2014. [Addendum: Phys. Rev.C90,no.3,039901(2014)].

[11] A. Kim *et al.*, "Target and Double Spin Asymmetries of Deeply Virtual π^0 Production with a Longitudinally Polarized Proton Target and CLAS," 2015.

[12] L. Favart, M. Guidal, T. Horn, and P. Kroll, "Deeply Virtual Meson Production on the nucleon," 2015.

[13] G. R. Goldstein, J. O. G. Hernandez, and S. Liuti, "Flavor dependence of chiral odd generalized parton distributions and the tensor charge from the analysis of combined π^0 and η exclusive electroproduction data," 2014.

[14] C. Lorce and B. Pasquini, "Quark Wigner Distributions and Orbital Angular Momentum," *Phys. Rev.*, vol. D84, p. 014015, 2011.

[15] I. C. Cloet, W. Bentz, and A. W. Thomas, "EMC and polarized EMC effects in nuclei," *Phys. Lett.*, vol. B642, pp. 210–217, 2006.

[16] E. R. Berger, F. Cano, M. Diehl, and B. Pire, "Generalized parton distributions in the deuteron," *Phys. Rev. Lett.*, vol. 87, p. 142302, 2001.

[17] A. Kirchner and D. Mueller, "Deeply virtual Compton scattering off nuclei," *Eur. Phys. J.*, vol. C32, pp. 347–375, 2003.

[18] M. Amarian *et al.*, "Deeply Virtual Compton Scattering on the Deuteron with CLAS at 6 GeV (PR12-06-015)," *A proposal to PAC 30*, 2006.

[19] R. B. Wiringa, R. Schiavilla, S. C. Pieper, and J. Carlson, "Nucleon and nucleon-pair momentum distributions in $A \leq 12$ nuclei," *Phys. Rev.*, vol. C89, no. 2, p. 024305, 2014.

[20] "CLAS12 Technical Design Report," 2008.

[21] J. Peyré, B. Genolini, and J. Poutas, "A Full-Scale Prototype for the Tracking Chambers of the ALICE Muon Spectrometer," 1998.

[22] T. Abe *et al.*, "Belle II Technical Design Report," 2010.

[23] E. Etzion *et al.*, "The Certification of ATLAS Thin Gap Chambers Produced in Israel and China," 2004.

[24] S. Biagi, "Monte Carlo simulation of electron drift and diffusion in counting gases under the influence of electric and magnetic fields," *Nucl.Instrum.Meth.*, vol. A421, pp. 234–240, 1999.

[25] M. Battaglieri *et al.*, "The Heavy Photon Search test detector," *Nucl.Instrum.Meth.*, vol. A777, pp. 91–101, 2015.

[26] T. C. Collaboration, "Clas12 forward tagger (ft) technical design report." https://www.jlab.org/Hall-B/clas12-web/docs/ft-tdr.2.0.pdf, 2012. Online; accessed 29 January 2016.

[27] K. Emi *et al.*, "Study of a dE/ dx measurement and the gas-gain saturation by a prototype drift chamber for the BELLE-CDC," *Nucl. Instrum. Meth.*, vol. A379, pp. 225–231, 1996.

[28] H. Fenker *et al.*, "BoNus: Development and use of a radial TPC using cylindrical GEMs," *Nucl. Instrum. Meth.*, vol. A592, pp. 273–286, 2008.

[29] M. Amaryan *et al.*, "The Structure of the Free Neutron at Large x-Bjorken (PR12-06-113)," *A proposal to PAC 30*, 2006.

[30] A. V. Belitsky and D. Mueller, "Refined analysis of photon leptoproduction off spinless target," *Phys. Rev.*, vol. D79, p. 014017, 2009.